atmosphere

MDPI

Article

Interannual Meteorological Forcing and Spatial Heterogeneity of Winter $PM_{2.5}$ Regimes in Central China

Yanhua He [1,2], Yan Yu [2,3], Xiawen Lei [1,2], Xiaoyong Liu [4], Fangcheng Su [1,2,*] and Ruiqin Zhang [1,2,*]

[1] School of Ecology and Environment, Zhengzhou University, Zhengzhou 450000, China; zzuhyh@gs.zzu.edu.cn (Y.H.)
[2] Research Institute of Environmental Sciences, Zhengzhou University, Zhengzhou 450000, China
[3] College of Chemistry, Zhengzhou University, Zhengzhou 450000, China
[4] School of Geographic Sciences, Xinyang Normal University, Xinyang 464000, China
* Correspondence: sufangcheng@zzu.edu.cn (F.S.); rqzhang@zzu.edu.cn (R.Z.)

Abstract

Despite substantial improvement in air quality in China, winter $PM_{2.5}$ concentrations particularly in January show limited decline, especially in the central region. This study used statistical analysis and WRF-CMAQ to examine how typical meteorological years affect transport and pollution processes in Henan. The mean effect difference ranged from −22 to 33%. In January 2020, weak winds and a low planetary boundary layer increased $PM_{2.5}$ by 3–33%, whereas in January 2023, stronger northerly winds and a higher boundary layer reduced $PM_{2.5}$ by 12–22%. These differences altered transport pathways, leading to a shift in dominant source regions from Beijing–Tianjin–Hebei and Shandong to Anhui and Hubei, with primary $PM_{2.5}$ showing high sensitivity to transport pathways, whereas secondary $PM_{2.5}$ remained relatively stable due to its dependence on regional chemical formation. Typical meteorological years in Henan exhibit two distinct pollution regimes: The local accumulation regime (2020) showed faster growth (20–30 μg m^{-3} d^{-1}), a higher peak (107 μg m^{-3}), longer persistence, and slower dissipation and was dominated by near-range transport. In contrast, the regional transport regime (2023) exhibited slower growth (<20 μg m^{-3} d^{-1}), a lower peak (99 μg m^{-3}), shorter persistence, and more rapid dissipation and was sustained by multi-regional input from Anhui, Shandong, and Hubei. In both episodes, primary $PM_{2.5}$ dominated during the growth and peak stages, whereas secondary $PM_{2.5}$ played a more prominent role during dissipation.

Keywords: $PM_{2.5}$; WRF-CMAQ; meteorological impacts; regional transport; Henan province

Check for updates

Academic Editor: Anil Namdeo

Received: 18 April 2026
Revised: 6 May 2026
Accepted: 12 May 2026
Published: 15 May 2026

Copyright: © 2026 by the authors. Licensee MDPI, Basel, Switzerland. This article is an open access article distributed under the terms and conditions of the Creative Commons Attribution (CC BY) license.

1. Introduction

$PM_{2.5}$ is one of the most harmful components of air pollution, with a diameter of 2.5 micrometers or less. It can remain suspended in the atmosphere for long periods, posing significant risks to human health, particularly respiratory and cardiovascular diseases [1,2]. Additionally, $PM_{2.5}$ has substantial ecological impacts, including altering nutrient balances, damaging vegetation, acidifying water bodies, and reducing visibility [3]. Since the implementation of China's 13th Five-Year Plan, air quality has improved substantially [4], but regional disparities remain pronounced [5]. Central China, represented by Henan Province, remains among the most polluted regions in the country. According to official ecological environment bulletins, the annual mean $PM_{2.5}$ concentrations in Henan, Hebei, and Shandong remained relatively high in 2024 [6–8]. $PM_{2.5}$ pollution during autumn and winter remains particularly severe, with frequent heavy pollution

episodes closely linked to meteorological conditions [9]. Under fixed emission scenarios, unfavorable meteorological conditions, such as low wind speed, temperature inversions, weak turbulence, and a shallow planetary boundary layer, inhibit atmospheric dispersion and enhance both primary $PM_{2.5}$ accumulation and secondary $PM_{2.5}$ formation [10,11]. Meanwhile, large-scale synoptic circulation can facilitate regional transport of pollutants from upwind areas to receptor regions, further intensifying pollution [12–14].

Generally, the emission baselines determine the long-term characteristics of pollution, while meteorological conditions influence pollution states by affecting boundary layer height, transport pathways, and other features. Numerous studies have quantitatively assessed the effects of meteorological factors on $PM_{2.5}$ pollution, such as low wind speed and a shallow boundary layer, promote $PM_{2.5}$ accumulation [15], whereas stronger ventilation and a deeper boundary layer facilitate the removal of pollutants [16]. Using a scenario analysis approach and comparing data from the winters of 2012 and 2013, Zheng et al. concluded that the key factor driving the heavy pollution event in Northeast China in 2013 was regional stable meteorological conditions, rather than a sudden increase in anthropogenic emissions [17]. Statistical methods such as multiple linear regression have been used to quantify the relationship between meteorological factors and $PM_{2.5}$ concentrations. For example, Wang et al. revealed a significant negative correlation between dynamic factors like wind speed and $PM_{2.5}$ levels [18]. In recent years, the gradient boosting machine technique has demonstrated that unfavorable meteorological conditions significantly increased $PM_{2.5}$ concentrations, leading to a 9% rise over the North China Plain compared to the same period from 2015 to 2019 [19]. Numerical simulations have also been widely used to quantify the relationship between meteorological variability and $PM_{2.5}$ concentrations, particularly through meteorology-chemistry coupled models such as WRF-Chem and CMAQ [20–22]. Using WRF-Chem, Li et al. [23] investigated the drivers of severe haze over the North China Plain in January 2020 and showed that, despite substantial emission reductions, interannual meteorological variability alone could cause $PM_{2.5}$ changes ranging from −13 to +15%. Using WRF-CMAQ, previous work simulating January and July 2013 showed that $PM_{2.5}$ was more sensitive to meteorological parameters in winter than in summer, with the strongest wintertime sensitivity to temperature, reaching $-5\ \mu g\ m^{-3}\ K^{-1}$ [22].

Meteorological variability often accompanies the interregional transport of pollutants. In quantitative studies of regional transport, numerical models represent one of the fundamental methods. For example, using PMF with FLEXPART-WRF to classify transport pathways and CAMx-PAST to quantify source contributions, researchers found that unfavorable meteorological conditions such as stable atmosphere and high humidity significantly enhanced regional transport, contributing up to 62% of $PM_{2.5}$ during the pollution accumulation stage [24]. Similarly, coupling WRF-CMAQ with the transport flux method and a regional transport matrix, studies show that meteorological conditions regulate the transport efficiency, with regional transport contributing 37–49% of $PM_{2.5}$ to four channel cities in the Beijing–Tianjin–Hebei region [25]. Using ISAM in the WRF-CMAQ model, researchers quantitatively calculated contributions from different source regions, further confirming the significant contribution (71%) of regional transport to $PM_{2.5}$ [26]. Several studies have confirmed the significant role of regional transport in $PM_{2.5}$ heavy pollution episodes. Research on severe haze in Beijing indicates that regional transport influences secondary $PM_{2.5}$ components more than local sources, contributing up to 60% during extreme events [27]. Hu et al. [28] reported that topography-enhanced regional transport significantly affected winter $PM_{2.5}$ levels in Henan, with contributions from neighboring air masses ranging from 40 to 50%, altering the pollution evolution process. A quantitative analysis of winter pollution in the Yangtze River Delta found that during peak pollution periods, inter-regional transport accounted for 70% of the total $PM_{2.5}$ concentration, while

local emissions contributed only 30%. This demonstrates that under stable meteorological conditions, inter-regional transport plays a dominant role in both pollution accumulation and peak stages [29]. Furthermore, meteorological conditions not only determine the intensity of regional transport but also shape its evolutionary patterns. For example, a study focusing on central China identified distinct regional transport types: rapid transit transport and stationary accumulation transport. Both types are triggered by strong northerly winds that transport high-$PM_{2.5}$ air masses southward and terminate rapidly due to cold fronts and or scavenging [30]. Under significant regional pollution, local emission reductions alone cannot effectively improve air quality; coordinated inter-regional efforts are necessary. Wang et al. [31] demonstrated through multi-scenario simulations that in the Beijing–Tianjin–Hebei region, local reductions contributed approximately 60% to $PM_{2.5}$ decreases, with coordinated regional reductions contributed about 40%. Li et al. [32] further showed that coordinating emission reductions in surrounding areas could additionally reduce $PM_{2.5}$ concentrations by 10–30%.

Recent studies in northern China have demonstrated that meteorological factors play a crucial role in shaping the temporal variability and spatial distribution of $PM_{2.5}$, with their influence becoming increasingly important under evolving emission conditions [33,34]. In the post-COVID-19 period, this issue has become more pronounced, as the recovery of precursor emissions combined with unfavorable meteorological conditions has led to a rebound in $PM_{2.5}$ pollution [16,35]. Against this background, although air quality in China has improved in recent years [36], such improvements have been uneven across seasons [37], and heavy pollution episodes remain frequent in winter, especially in January. Henan Province is one of the representative regions most severely affected by $PM_{2.5}$ pollution in China, with mean $PM_{2.5}$ concentrations in January consistently exceeding 70 $\mu g\ m^{-3}$, more than twice the interim target concentration limit, and often reaching moderate to heavy pollution levels, despite regional reductions in precursor emissions [38]. High-intensity emissions from winter heating, industry, and motor vehicles provide an inherent basis for regional $PM_{2.5}$ pollution [39,40], yet the pollution still exhibits strong meteorology-driven characteristics [41]. In this study, statistical analysis and numerical modeling were combined to examine the impacts of meteorological variability on $PM_{2.5}$ concentrations in Henan Province during January from 2015 to 2025. By incorporating inter-city variability, it also reveals the spatial heterogeneity of meteorological effects, providing new insights into the uncertainty and regional differences in pollution processes. Typical years and representative pollution episodes were selected to quantify the contributions of local emissions and interprovincial transport. Furthermore, this study identifies distinct meteorological regimes and their associated pollution mechanisms. Thereby supporting more targeted winter air-pollution control strategies in Henan Province.

2. Methodology

2.1. Data Source

The study period covered 2015–2025. Observational data were obtained from the national air-quality monitoring stations in Henan Province (https://sthjt.henan.gov.cn/, accessed on 5 April 2025), and city-level mean concentrations were calculated after removing invalid and negative values to represent urban pollution levels. Meteorological observations were obtained from the official website of the Henan Provincial Meteorological Bureau (https://www.weather.com.cn/weather/101180101.shtml, accessed on 5 April 2025). The meteorological reanalysis data used to drive the WRF model were the Final Operational Global Analysis (FNL) data from the National Centers for Environmental Prediction (NCEP, https://gdex.ucar.edu/datasets/d083002/, accessed on 5 April 2025) [42]. Anthropogenic emissions were taken from the Multi-resolution Emission Inventory for China (MEIC)

developed by Tsinghua University [43], while biogenic emissions were generated using the MEGAN v2.1 model [44].

The emission inventory used in this study covered all of China with a horizontal resolution of 36 km. During emission processing, emissions from Henan Province, its surrounding provinces, and the rest of China were tagged separately (Figure S1) to better characterize pollutant transport between Henan and surrounding regions, as well as the contributions of different source regions to air pollution in Henan. In the source-tagging analysis, Henan and the surrounding regions were defined as follows: natural sources (R0), Henan (R1), Hebei (R2), Beijing and Tianjin (R3), Shaanxi (R4), Shanxi (R5), Hubei (R6), Shandong (R7), Anhui (R8), and other regions (R9).

2.2. Research Methods

2.2.1. WRF-CMAQ Model Setup

This study used WRF v4.13 was driven by NCEP FNL reanalysis data and configured with 30 vertical layers, and CMAQ v5.3.1 (the SAPRC07 photochemical mechanism for gas-phase chemistry, the AERO6 aerosol module, and the M3Dry bidirectional dry deposition model). The modeling domain covered all of China (Figure S1) with a horizontal resolution of 36 km and 160 × 130 grid cells. Simulations were conducted for January of 2015–2025, with year-specific WRF meteorological fields and emission inventories. Each simulation included a 5-day spin-up period, and the initial and boundary conditions were gradually provided by the outer domain to minimize the influence of the initial fields on the inner-domain results [45]. Detailed model settings and the physical and chemical schemes are described in Ref. [46]. Based on this setup, a source-oriented CMAQ model was developed to apportion primary particulate matter (PPM), secondary inorganic aerosol (SIA), and secondary organic aerosol (SOA). This source-tagging framework was used not only to quantify regional source contributions but also to examine how different meteorological backgrounds modified transport pathways and source-contribution structures. PPM was tracked using chemically inert tracers released from each source at 0.001% of the corresponding PPM emission rate. These tracers underwent transport and deposition processes only and did not affect aerosol chemistry [47]. Their simulated concentrations were then scaled to derive source contributions to PPM. SIA and SOA were tracked by tagging gaseous precursors emitted from different regions within the chemical mechanism. During subsequent gas-phase reactions, aerosol chemistry, and gas-particle conversion, the resulting secondary products inherited the source labels [48], enabling full-process attribution of secondary aerosol formation. Further methodological details are available in Ying et al. [49]. In total, 10 emission sources were tagged, and the tracer labels X0 and X2–X9 were appended to precursor names during emission processing.

2.2.2. Model Validation Methods

In this study, the performance of the WRF model in simulating the meteorological fields during pollution episodes was evaluated using temperature, relative humidity, pressure, and wind speed. CMAQ-simulated air pollutant concentrations were assessed against observational data. The statistical metrics used for model evaluation included mean bias (MB), mean absolute gross error (MAGE), root mean square error (RMSE), mean fractional bias (MFB), mean fractional error (MFE), and the correlation coefficient (R), as shown in Table S1.

2.2.3. Quantification of Meteorological and Emission Effects

This study used a sensitivity simulation with fixed emissions and varying meteorological fields. The WRF model provided year-specific meteorological fields for 2015–2025, while the 2020 local emission inventory for Henan Province remained unchanged. Under this

framework, variations in simulated $PM_{2.5}$ reflect only meteorological variability, allowing its effect on $PM_{2.5}$ concentrations to be quantified. January 2016 is taken as an example:

$$n = \frac{p' - p}{p} \times 100\% \quad (1)$$

In the equations, n denotes the anomaly and represents the effect of meteorological change on $PM_{2.5}$ concentrations in Henan Province in January 2016 (%). Positive values indicate more unfavorable meteorological conditions, whereas negative values indicate more favorable conditions. p' denotes the simulated monthly mean $PM_{2.5}$ concentration (μg m^{-3}) in Henan Province in January 2016, and p denotes the mean simulated monthly $PM_{2.5}$ concentration (μg m^{-3}) in January during 2015–2025.

Variations in $PM_{2.5}$ concentrations reflect the combined influences of source emissions and meteorological conditions. The quantitative approach used to assess the annual contributions of emissions and meteorology is described below

$$D_2 = \frac{\frac{O_{2016}-O_{2020}}{O_{2020}} - \left(\frac{M_{2016}E_{2020}-M_{2020}E_{2020}}{M_{2020}E_{2020}}\right)}{1 + \left(\frac{M_{2016}E_{2020}-M_{2020}E_{2020}}{M_{2020}E_{2020}}\right)} \quad (2)$$

$M_{2020}E_{2020}$ denotes the simulated $PM_{2.5}$ concentration under 2020 emissions and 2020 meteorological conditions, and $M_{2016}E_{2020}$ denotes the simulated $PM_{2.5}$ concentration under 2020 emissions and 2016 meteorological conditions. $D_1 = (M_{2016}E_{2020} - M_{2020}E_{2020})/M_{2020}E_{2020}$ therefore represents the year-on-year change in $PM_{2.5}$ driven by meteorological variation after removing the effect of emission changes. Positive values indicate unfavorable meteorological conditions, whereas negative values indicate conditions favorable for dispersion. Observed $PM_{2.5}$ concentration changes reflect the combined effects of meteorology and emissions. We define the relative change as $D_3 = (O_{2016} - O_{2020})/O_{2020}$ where O_X denotes the observed $PM_{2.5}$ concentration in year X. Accordingly, D_1 represents the year-on-year change attributable to meteorology, D_2 represents the year-on-year change attributable to emissions, and D_3 represents the observed concentration change. Previous studies have widely applied this method [50,51]. Compared with simple substitution of meteorological and emission conditions, this method quantifies their respective effects on $PM_{2.5}$ more accurately.

3. Results and Discussion

3.1. Model Validation

The WRF model shows good performance in simulating winter meteorological variables over Henan Province, as evaluated against observations for January 2020 and January 2023 (Figure S2; Table S2). For temperature, the model captures the day-to-day variations well, with R of 0.79 (2020) and 0.87 (2023). A slight warm bias is evident, with MB of +0.95 °C (2020) and −0.12 °C (2023). For wind speed, the model reproduces the observed fluctuations (e.g., around 5 January 2020 and 20 January 2023), with R of 0.77 (2020) and 0.79 (2023); the MB are 0.17 m s^{-1} and 0.47 m s^{-1}, respectively. Relative humidity simulations show larger discrepancies, with MB of −14.19% (2020) and −2.07% (2023), likely related to uncertainties in precipitation. Air pressure is well simulated, with an R of 0.97 (2020) and 0.77 (2023). Overall, the modeling system meets the performance criteria recommended by Emery et al. [52] for most variables, except for temperature MB, which slightly exceeds the ±0.5 °C threshold but remains within the less stringent criterion of McNally et al. [53] (MB ≤ ±1.0 °C). The model therefore provides a reliable meteorological basis for subsequent air quality simulations.

For pollutant validation, January 2020 was selected because the 2020 emission inventory was used as the baseline emission input in this study. Under this condition, the simulated pollutant concentrations and observed pollutant concentrations correspond to the same emission year and meteorological year, allowing a more consistent evaluation of CMAQ model performance. Figure 1 and Table S2 compare the simulated and observed concentrations of major pollutants in Henan Province in 2020. The WRF-CMAQ model captured the January variations in major pollutants well, with good overall correlations. For daily $PM_{2.5}$, the MFB and MFE were −0.06 and 0.22, respectively, with a correlation coefficient of 0.73. For daily PM_{10}, the corresponding values were 0.06 and 0.14, respectively, with a correlation coefficient of 0.75, meeting the criteria proposed by Boylan and Russell [48]. For gaseous pollutants, the evaluation based on NMB and NME indicates that $|NMB| \leq 15\%$ and $NME \leq 35\%$ define the Performance Goal, whereas $|NMB| \leq 30\%$ and $NME \leq 75\%$ indicate the Performance Criteria. SO_2 and NO_2 were generally within the Performance Goal range, with NMB values of 0.08 and 0.14, NME values of 0.14 and 0.15, and correlation coefficients of 0.76 and 0.95, respectively. The R values for all pollutants were above 0.70, indicating satisfactory model performance.

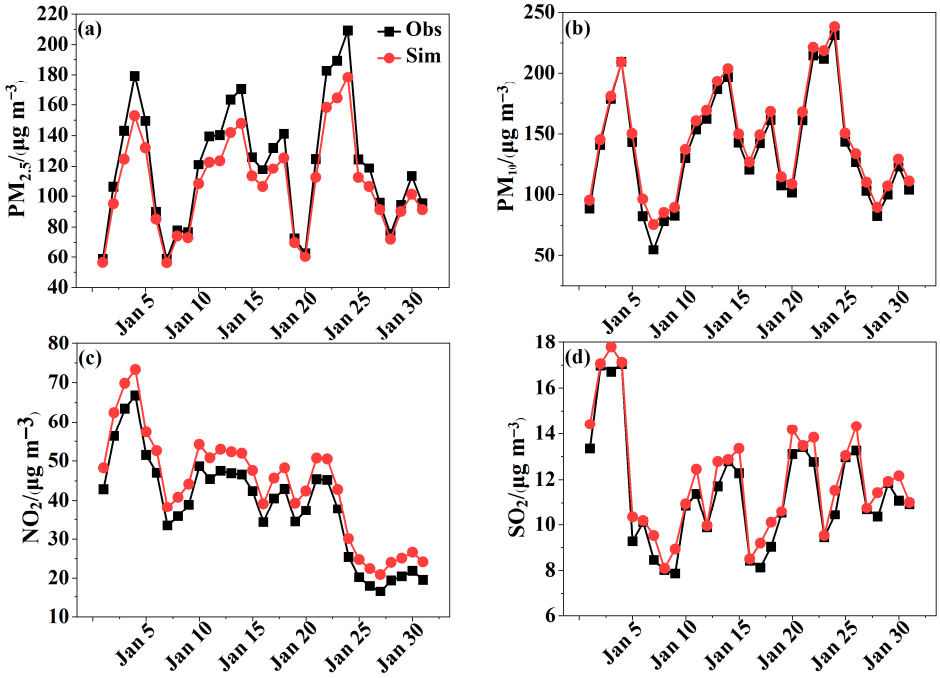


Figure 1. Model simulation vs. observation of pollutants in Henan Province (January 2020), (**a**) $PM_{2.5}$; (**b**) PM_{10}; (**c**) NO_2; (**d**) SO_2.

In summary, the WRF model reasonably reproduced the main meteorological conditions in the two representative months, and the CMAQ model showed acceptable performance in simulating $PM_{2.5}$, PM_{10}, SO_2, and NO_2 under the 2020 baseline emission scenario. Although some uncertainties remain, especially in the simulation of relative humidity, the overall validation results indicate that the WRF-CMAQ modeling system can provide a reliable basis for the subsequent analyses of meteorological effects, source contributions, and regional transport.

3.2. Evolution and Impact Characteristics of Key Factors

The WRF model captures the interannual variability of winter meteorological conditions in Henan Province. Figure 2 shows the January mean wind field, boundary layer height, and $PM_{2.5}$ concentration in Henan Province and surrounding regions from 2015 to

2025. Boundary layer height shows clear interannual variability, ranging from 250 to 400 m. It reaches a maximum in 2016 (396 m) and a minimum in 2020 (270 m), with a difference of more than 120 m. During 2017–2019, boundary layer height remains below 350 m, and during 2021–2025 it increases first and then fluctuates. Spatially, low values (≤300 m) occur mainly in the northwest, west, and south, whereas high values (>300 m) concentrate in the northeast and eastern plains. Wind speed also shows marked interannual variation, with the mean value reaching a maximum in 2025 (4 m s^{-1}) and a minimum in 2019 (1 m s^{-1}). Since 2020, the annual mean wind speed has remained above 3 m s^{-1}. Wind direction indicates that northerly, northeasterly, and northwesterly winds prevail in winter over Henan Province, favoring persistent transport of pollutants from northern regions.

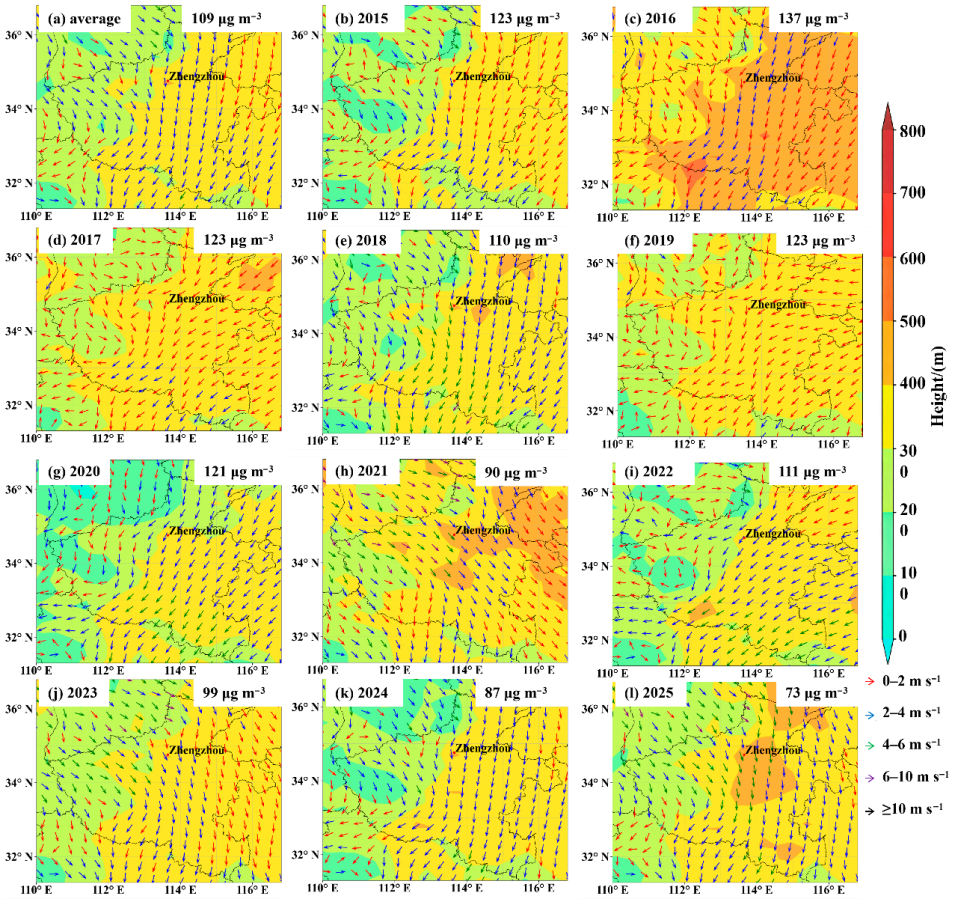


Figure 2. Interannual variation of boundary layer height and wind field over Henan Province in January (2015–2025).

The boundary layer height and wind speed jointly control $PM_{2.5}$ dispersion. In winter, a lower boundary layer and weaker winds enhance $PM_{2.5}$ accumulation [54]. High $PM_{2.5}$ further suppresses boundary layer development through radiative effects, and low wind speed intensifies near-surface accumulation [55]. Based on the coupling of boundary layer height and wind speed, the study years were classified into high-concentration years (2016, 2017, 2019, and 2020) and low-concentration years (2021, 2023, and 2025). High-concentration years show unfavorable coupling, but with different dominant mechanisms. In 2016, 2017, and 2019, boundary layer height exceeds 300 m, whereas wind speed remains at 0–2 m s^{-1} over most of Henan Province, indicating weak horizontal transport. In 2020, wind speed reaches 3 m s^{-1}, but boundary layer height drops to the study-period minimum (270 m), indicating a negative relationship between boundary layer height and $PM_{2.5}$. Low-concentration years show favorable coupling, with wind speeds above 3 m s^{-1}, consistent

northerly to northwesterly flow, and relatively high boundary layers. These conditions favor horizontal transport and vertical dispersion, thereby reducing $PM_{2.5}$. This pattern agrees with results from the North China Plain, where pollution episodes often end with stronger winds and a higher boundary layer [56].

3.3. Quantitative Effects of Meteorological Conditions on $PM_{2.5}$

Under fixed emissions and varying meteorological fields, Figure 3 shows the effects of meteorological conditions on January $PM_{2.5}$ from 2015 to 2025. The blue line represents the mean effect difference, which is used for the following analysis. The black line indicates the spatial mean of meteorological effect differences across cities, with error bars representing the standard deviation. The meteorological effect difference for each city was calculated using Equation (2). Results are shown in Table S3. The error bars reflect the spatial variability among cities and provide an indication of uncertainty. Positive values indicate conditions unfavorable for dispersion, whereas negative values indicate conditions favorable for dispersion and removal. The annual meteorological effect ranged from −22 to 33%, indicating marked interannual variability. Notably, the presence of error bars suggests that meteorological effects exhibit spatial heterogeneity across cities. Three periods were identified. The unfavorable period was represented by 2020, with a domain-averaged effect difference of +33%. Stagnant meteorological conditions dominated during this year, and $PM_{2.5}$ reached 64 μg m^{-3}, well above the multi-year mean of 48 μg m^{-3}. Both 2019 and 2022 also showed positive values exceeding +10%. The favorable period was represented by 2023, with an effect difference of −22%. Favorable dispersion conditions, such as cold-air activity, reduced $PM_{2.5}$ to 37 μg m^{-3}, below the multi-year mean. In 2025, the annual mean effect difference was also below −10%. The corresponding error bars suggest relatively small inter-city variability during this period. The neutral period included 2015–2018, during which the domain-averaged effect differences remained within ±10%. The error bars indicate that spatial variability during this period was greater than that observed in favorable years.

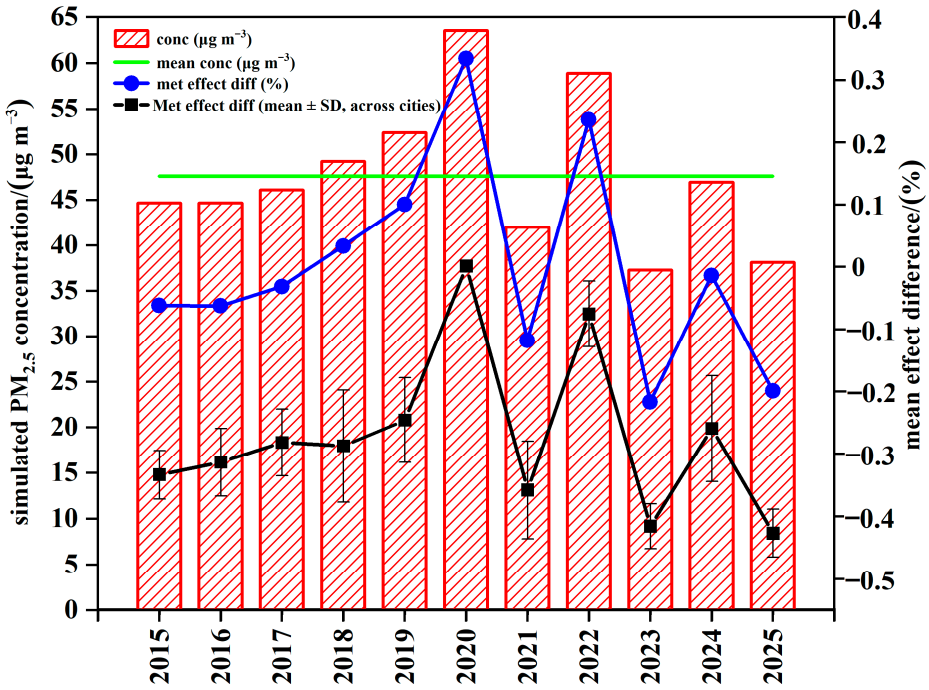


Figure 3. Interannual variation in simulated January $PM_{2.5}$ concentrations and mean effect differences. from 2015 to 2025.

3.4. Spatial Variation in Meteorological Effects

At the provincial scale, interannual $PM_{2.5}$ variation is jointly driven by meteorology and emissions. Figure 4, Figures S3 and S4 shows the emission effect, meteorological effect, and year-on-year $PM_{2.5}$ change across 17 cities in Henan Province (excluding Jiyuan). Positive emission effects indicate weaker control, whereas negative values indicate stronger control. Positive meteorological effects indicate conditions unfavorable for dispersion, whereas negative values indicate favorable dispersion.

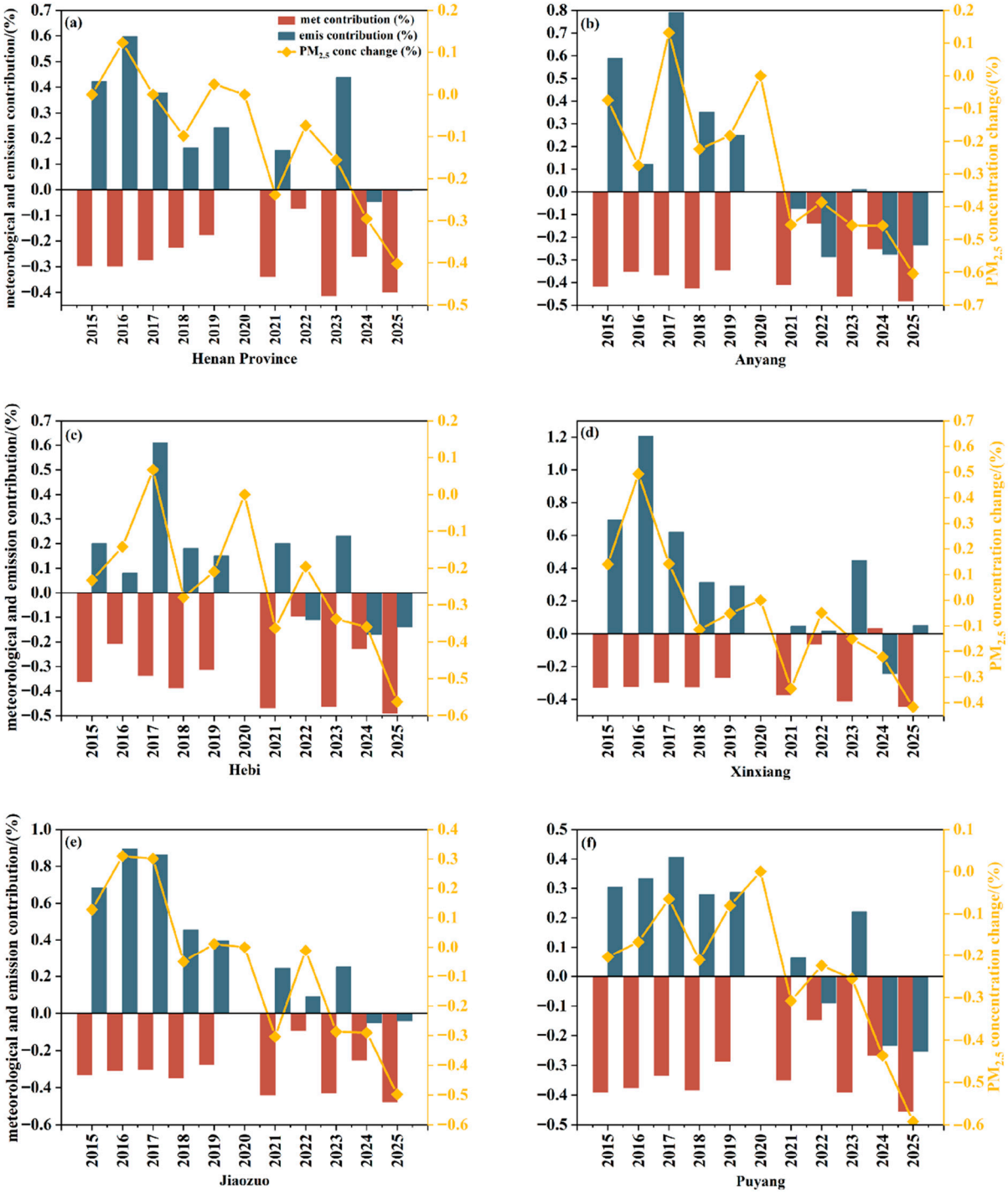


Figure 4. Interannual changes in meteorological effect, emission effect, and $PM_{2.5}$ concentration across cities in Henan Province during January 2015–2025, (**a**) Henan Province; (**b**) Anyang; (**c**) Hebi; (**d**) Xinxiang; (**e**) Jiaozuo; (**f**) Puyang.

We quantify the relative contributions of meteorology and emissions to $PM_{2.5}$ variability. Figure 4a shows marked interannual variability. Meteorological effects vary by 41% and are mostly negative, whereas emission effects vary by 64% and are mostly positive.$PM_{2.5}$ changes range from −40 to +12%, indicating large combined effects of meteorology and emissions, consistent with Huang et al. [57,58]. For example, favorable meteorology (–30%) fails to prevent a 12% increase in $PM_{2.5}$ because emissions rise sharply (+60%). In 2025, $PM_{2.5}$ decreases by 40%, driven by favorable meteorology and emission reduction (–0.3%). Interannual variations for each city are shown in Table S4.

The range of year-on-year $PM_{2.5}$ changes under meteorological effects (maximum minus minimum) reflects city-level sensitivity to meteorological variability; a larger range indicates a stronger response [59]. As shown in Figure 4, Figures S3 and S4, high sensitivity (>47%) occurs in northern cities such as Anyang, Hebi, and Xinxiang; moderate sensitivity (40–45%) in Puyang, Zhengzhou, and Kaifeng; and low sensitivity (<40%) in southern cities such as Xinyang. For emission effects, all cities show positive year-on-year values during 2015–2019. During 2021–2025, northern Henan shows values below −10%, indicating strong emission reduction; central Henan ranges from −5 to 5%, indicating moderate reduction; and southern Henan exceeds 1%, indicating emission growth. Overall, three types emerge: high sensitivity-strong reduction in northern Henan, moderate sensitivity-moderate reduction in central Henan, and low sensitivity-weak reduction in southern Henan.

Northern Henan cities (high sensitivity, strong emission reduction) are located in industrial clusters. Their meteorological sensitivity exceeds 47%. During 2015–2019, emission effects are mostly positive (20–45%), indicating strong industrial emissions. During 2021–2025, they turn negative, reaching −24% in Anyang, −14% in Hebi, and −25% in Puyang in 2025. Strong emission reduction drives a marked decline in $PM_{2.5}$, with decreases of −60% in Anyang and −56% in Hebi, and generally over 45%.

Central Henan cities, characterized by moderate sensitivity and moderate emission reduction, show meteorological effects of −25 to −45%. In Zhengzhou, the value ranges from −5% in 2022 to −43% in 2025, and in Kaifeng from −11 to −44%. Emission effects are mostly positive during 2015–2019, but turn slightly negative in some years after 2021, remaining weaker than in northern Henan. $PM_{2.5}$ declines by 30–45%, including −45% in Zhengzhou and −42% in Kaifeng, lower than in northern Henan.

Southern Henan cities, characterized by low sensitivity and weak emission reduction, show meteorological effect ranges below 40%. In Xinyang, the value ranges from −2% in 2022 to −39.2% in 2023, and in Zhumadian from −4 to −43%. Emission effects remain positive during 2021–2025, indicating persistent emission pressure. $PM_{2.5}$ declines only modestly, by −17% in Xinyang, −18% in Nanyang, and −28% in Zhumadian, all lower than in northern and central Henan.

3.5. Meteorological Effects on Typical Pollution Episodes

To further move beyond a descriptive comparison of pollution levels, we investigated the transport pathways, source contribution structures, and process evolution of winter $PM_{2.5}$ pollution under different meteorological backgrounds. The analysis focused on the influence of typical meteorological years on regional transport pathways and source contributions, as well as the stage-dependent evolution of heavy pollution episodes. Particular attention was also given to the different responses of primary and secondary $PM_{2.5}$.

3.5.1. Regional Transport Characteristics in Typical Meteorologically Influenced Months

To examine the effects of meteorology on pollution characteristics, we selected 2020 (most unfavorable meteorology) and 2023 (most favorable meteorology) as typ-

ical years. Meteorological conditions reshape regional transport by regulating transport pathways and dispersion capacity (Table S5). In January 2020, local contributions accounted for 21%, while regional transport contributed 76%, in the order of Beijing–Tianjin–Hebei > Shandong > Shanxi > Anhui. In January 2023, the local contribution increased to 25%, regional transport contributed 73%, with the order shifting to Anhui > Shandong > Hubei > Beijing–Tianjin–Hebei. In 2020, persistent northeasterly winds and relatively strong wind speed (3 m s^{-1}) enhanced low-level transport from Beijing–Tianjin–Hebei, Shandong, and Shanxi, increasing the regional contribution. In 2023, higher boundary layer height (341 m) and mean wind speed (3 m s^{-1}) strengthened vertical and horizontal dispersion, thereby reducing the regional contribution. Meanwhile, the meteorological field also changed (Figure 2). Airflow of 2–4 m s^{-1} over central and southwestern Henan favored local dispersion, whereas weak winds of 0–2 m s^{-1} over southeastern Henan highlighted inflow from Anhui, which became an important external source in 2023.

In 2020 and 2023, the source structures of primary and secondary $PM_{2.5}$ showed a consistent shift: contributions from traditional high-emission regions such as Beijing–Tianjin–Hebei and Shandong declined, whereas those from Henan and from the Anhui and Hubei directions increased, indicating a systematic adjustment in regional transport. Spatially, primary $PM_{2.5}$ closely matches total $PM_{2.5}$ and shows concentrated high-value areas, whereas secondary $PM_{2.5}$ shows a more uniform pattern, reflecting differences in formation mechanisms and transport scales. Primary $PM_{2.5}$ depends strongly on atmospheric dynamics. Its local contribution increased from 23 to 27%, whereas the regional transport contribution decreased from 78 to 74%. The dominant source regions shift from Shandong (18%) and Beijing–Tianjin–Hebei (16%) to Anhui (18%) and Hubei (13%), indicating a transport shift from north to south, likely driven by changes in winter circulation and wind fields. Figure 5 shows a stable spatial pattern in both years, with high values concentrated in major emission regions such as Beijing–Tianjin–Hebei and Henan, highlighting the strong constraint of emission source distributions on primary $PM_{2.5}$.

Secondary $PM_{2.5}$ shows clear regional chemical coupling. The local contribution rises to 23.0%, while regional transport still dominated (71%). the national background region (R9) remains high at 17% and 20%, indicating strong regional mixing and long-range precursor transport. The contribution from Beijing–Tianjin–Hebei declines from 20 to 12%, likely because weaker transport and a higher boundary layer enhance vertical dilution. Figure 5 shows that in 2023, secondary $PM_{2.5}$ extended from the North China Plain to the Fenwei Plain, the Middle and Lower Yangtze Plain, and the Sichuan Basin, reflecting larger-scale mixing [21,48]. In 2020, a lower boundary layer strengthens near-surface accumulation and secondary formation, producing a different spatial distribution.

Meteorological changes affect not only $PM_{2.5}$ concentrations but also regional contribution patterns. As conditions shift from unfavorable to favorable, dispersion improves and regional, especially long-range, transport weakens. Figure 6 shows interannual differences in within- and cross-province contributions to $PM_{2.5}$ across provinces. In 2020, under severe pollution and stagnant conditions, Beijing–Tianjin–Hebei exported substantial $PM_{2.5}$ to surrounding regions, contributing 37%, 24%, and 18% to Shandong, Shanxi, and Henan, respectively. By contrast, contributions to more distant provinces such as Shaanxi, Hubei, and Anhui reached only 8%, showing clear distance decay. In 2023, improved dispersion reshaped regional transport. External input declined, local contributions increased, and stronger atmospheric disturbance promoted multidirectional dispersion. Henan's contributions to Shanxi, Beijing–Tianjin–Hebei, and Shandong rose to 9%, 3%, and 8%, respectively, shifting Henan from a receptor to an exchange node. Meanwhile, stronger turbulence and

horizontal dispersion weakened long-range export from Beijing–Tianjin–Hebei to Shaanxi, Hubei, and Anhui.

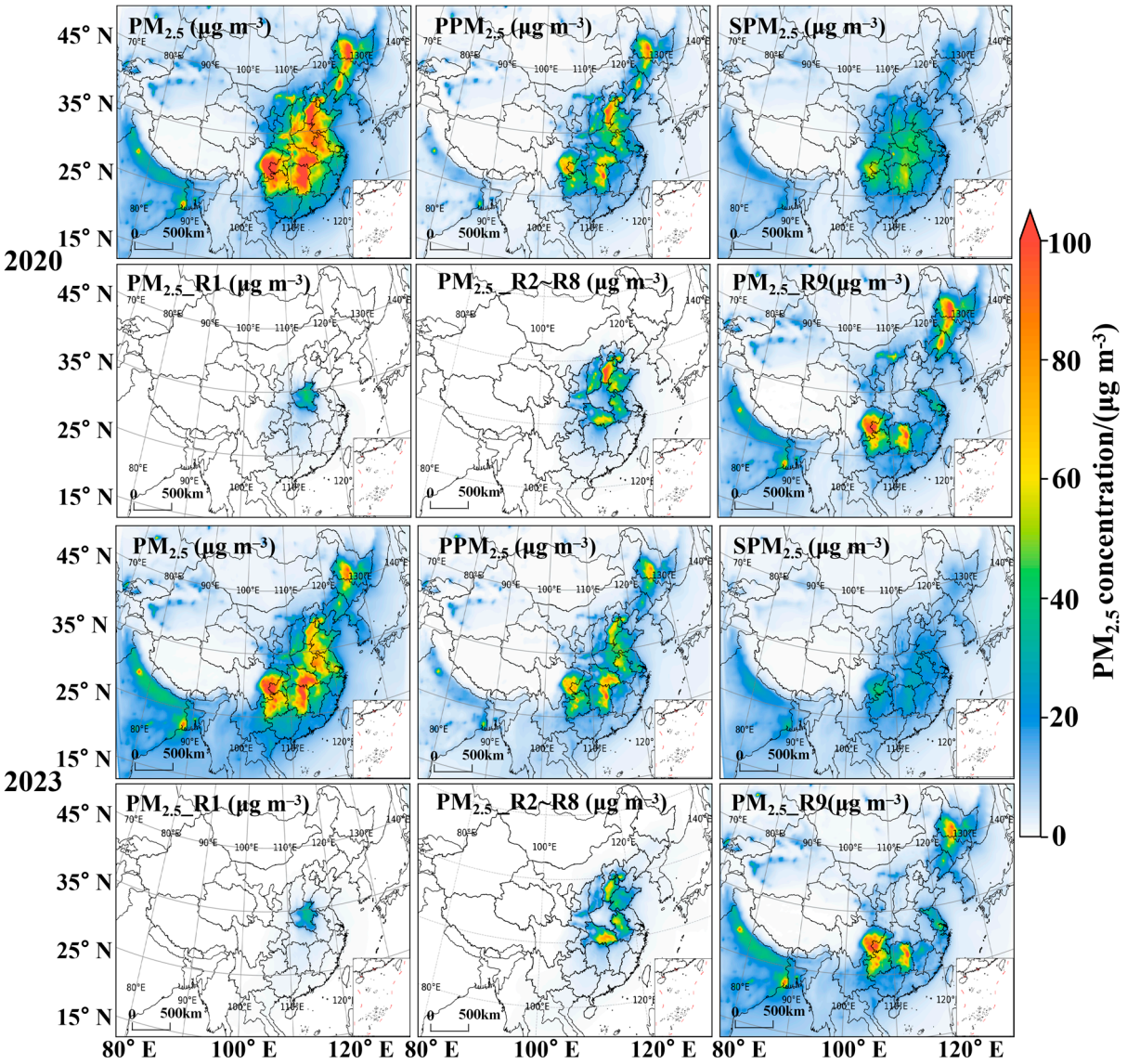


Figure 5. Source apportionment of $PM_{2.5}$ and its components in Henan Province (2020, 2023).

3.5.2. Regional Transport Characteristics During Typical Heavy Pollution Episodes

To investigate the evolution of different pollution types driven by meteorology, this study selected two typical heavy pollution episodes, 19–24 January 2020 and 9–14 January 2023, dividing each into accumulation, peak, and dissipation phases. This stage-based comparison not only explains the influence of meteorological conditions on pollution levels but also clarifies their effects on the $PM_{2.5}$ growth rate, peak intensity, pollution duration, removal process, and corresponding changes in source contributions. Results show that different meteorological conditions shift winter $PM_{2.5}$ pollution in Henan from local accumulation to regional transport.

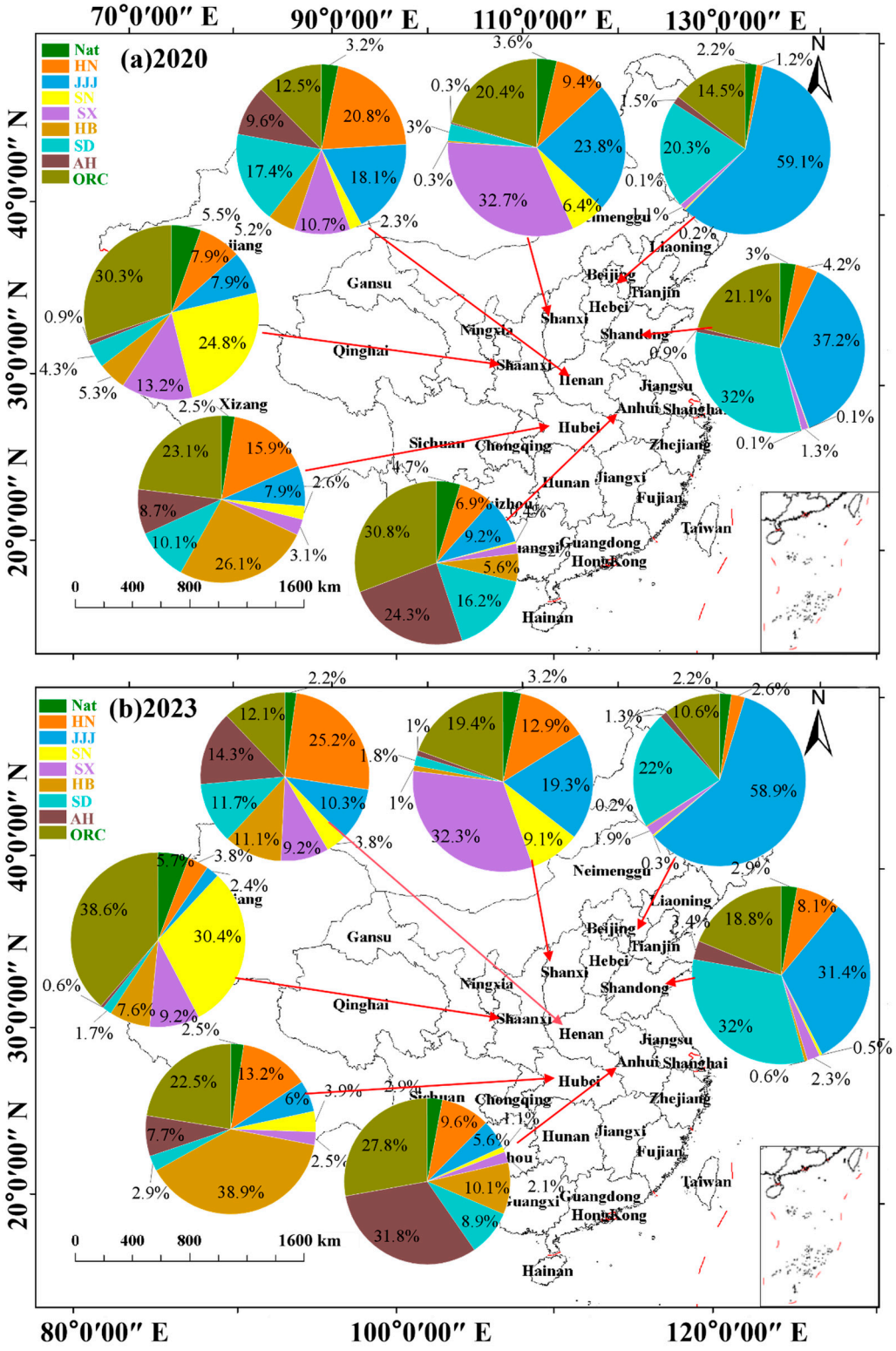


Figure 6. Source apportionment of $PM_{2.5}$ concentration: local vs. regional transport by province (2020, 2023).

In 2020, stagnant conditions suppressed dispersion and produced a local accumulation regime (Figure 7). Pollution initially developed in eastern and southeastern Henan, mainly from local sources, with additional input from Anhui and Shandong. Persistent unfavorable meteorology then strengthened regional transport and secondary formation, and $PM_{2.5}$ peaked at 107 μg m^{-3} on 22 January. Cold air then cleared pollution from north to south

and reduced $PM_{2.5}$ to 53 μg m^{-3} on 24 January. In 2023, the episode remained weaker but showed a stronger transport-driven regime. During the accumulation stage, air masses from the Hubei–Anhui region and Beijing–Tianjin–Hebei affected Henan simultaneously and brought strong external input. As pollution intensified over North China, regional transport increased, and $PM_{2.5}$ peaked at 99 μg m^{-3} on 12 January. Cold air then rapidly removed pollutants, although eastern and southeastern Henan responded more slowly, and $PM_{2.5}$ fell to 18 μg m^{-3} on 14 January. This result indicates that improved dispersion conditions enhance the relative contribution of regional transport in Henan.

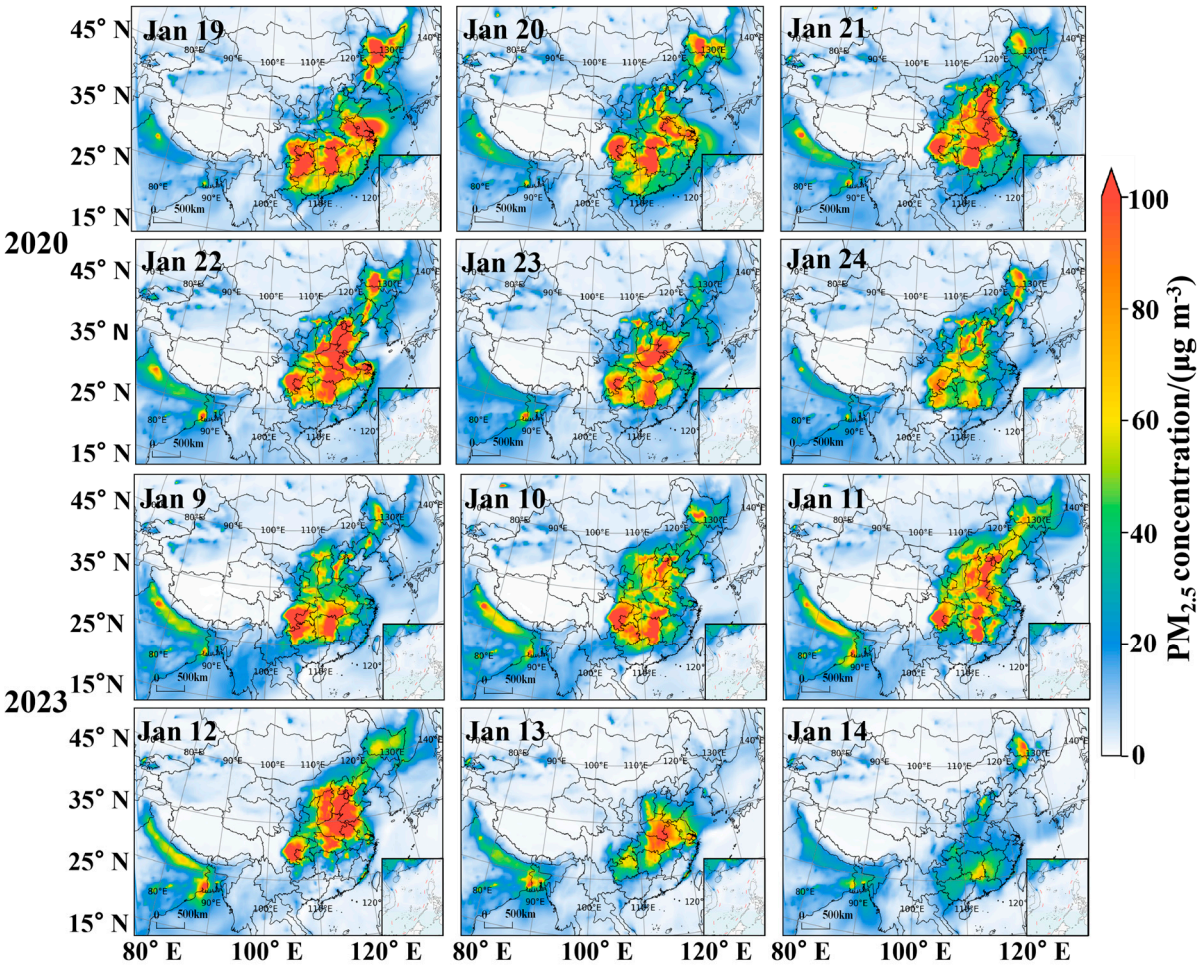


Figure 7. Spatial distribution during typical heavy pollution episodes (2020, 2023).

Among the two heavy pollution episodes, the local accumulation type shows a higher peak than the regional transport type. It occurs under a lower boundary layer, weaker winds, and weaker wind shear (Figure S5), which favor in-province accumulation. By contrast, the regional transport type occurs under a higher boundary layer, stronger winds, and better vertical mixing, which favor external input. Figure 8 highlights these differences. In 2020, local sources contributed 26% during the accumulation stage, and nearby precursor conversion raised $PM_{2.5}$ to 56 μg m^{-3}. At the peak stage, the local contribution rose to 26%, long-range input increased to 17%, and $PM_{2.5}$ reached 107 μg m^{-3}. During dissipation, cold-front passage increased the contributions from Shandong and Beijing–Tianjin–Hebei to 20% and 19%, while $PM_{2.5}$ fell to 53 μg m^{-3}. In 2023, local contributions remained lower, at 24% during accumulation and 22% at the peak, whereas long-range transport and input from Shandong, Anhui, and Hubei played larger roles, with $PM_{2.5}$ peaking at 99 μg m^{-3}.

During dissipation, cold air and wet deposition rapidly reduced $PM_{2.5}$ to 20 μg m^{-3}, with clear shifts in external contributions.

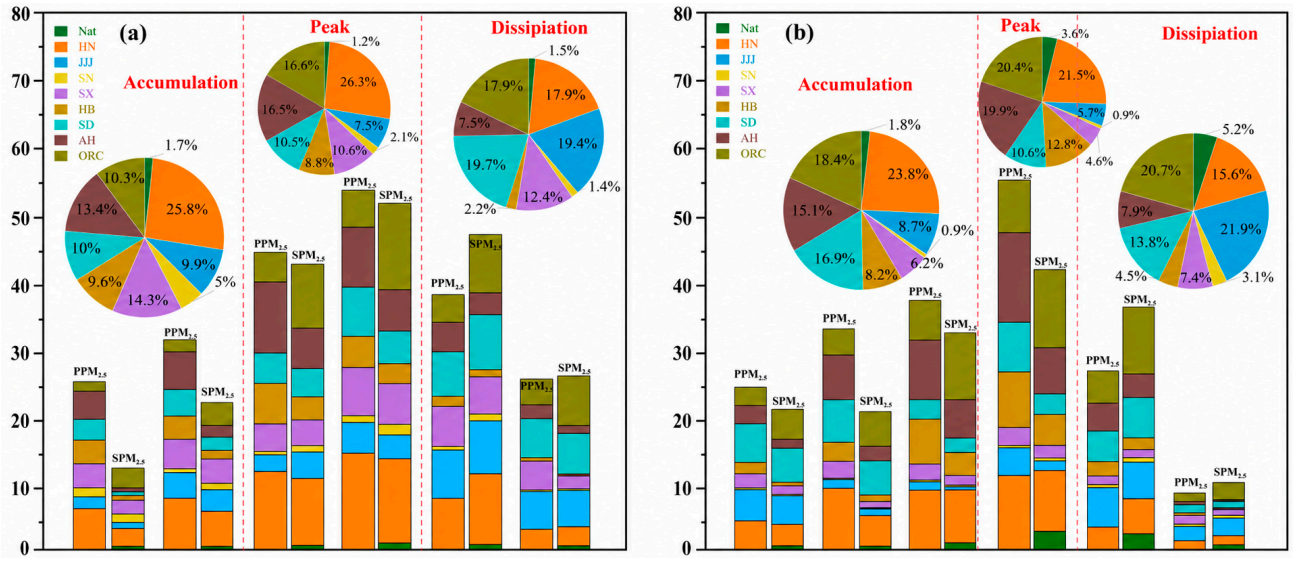


Figure 8. Source apportionment by region during typical heavy pollution episodes (2020, 2023), (**a**) typical episode in 2020; (**b**) typical episode in 2023.

In both years, primary and secondary $PM_{2.5}$ exhibited distinct source-contribution responses under different meteorological backgrounds. From accumulation to peak, primary $PM_{2.5}$ exceeds secondary $PM_{2.5}$, indicating dominant physical accumulation. During dissipation, secondary $PM_{2.5}$ surpasses primary $PM_{2.5}$ because precursor conversion continues. Figure 8 further shows that meteorology regulates the source structure of primary $PM_{2.5}$ In 2020, near-range transport dominated: under stagnant conditions, local sources (28%) and Anhui (24%) together contributed more than 50%, raising $PM_{2.5}$ to 55 μg m^{-3} and highlighting dominant local influence under weak winds. In 2023, stronger winds and vertical mixing produced a broader source pattern, with contributions from local sources (25%), Anhui (24%), Shandong (16%), and Hubei (10%). During dissipation in both years, the contribution from Beijing–Tianjin–Hebei increased sharply, reaching 22% in 2020 and 24% in 2023, indicating upstream transport with passing clean air masses.

In contrast, secondary $PM_{2.5}$ showed a more regionally mixed source-contribution pattern. Its response was not controlled only by physical transport, but also by precursor transport, regional chemical transformation, and gas-particle conversion. In 2020, local sources remained stable and near-range transport dominated. Local contributions averaged 23%, whereas Shanxi contributed 7–16%, with only small day-to-day variation, indicating dominant local and nearby conversion under stagnant conditions. In 2023, improved dispersion reduced the local contribution to 19%, whereas long-range transport became dominant at 25% on average. Contributions from Beijing–Tianjin–Hebei, Shandong, and Anhui varied more strongly, indicating greater dependence on long-range transport and regional chemical transformation.

4. Conclusions

This study quantified the effects of meteorological variability on winter $PM_{2.5}$ pollution in Henan Province using statistical analysis and WRF-CMAQ simulations for January during 2015–2025. By combining fixed-emission sensitivity simulations and source-oriented CMAQ modeling, we further examined how different meteorological backgrounds modi-

fied $PM_{2.5}$ concentrations, transport pathways, source-contribution structures, and heavy pollution evolution processes.

1. Winter meteorological conditions exerted a substantial influence on $PM_{2.5}$ concentrations in Henan Province. Under the fixed-emission framework, the mean meteorological effect difference ranged from −22 to +33%, indicating strong interannual variability. January 2020 represented the most unfavorable meteorological year, with a mean effect difference of +33%, while January 2023 represented the most favorable meteorological year, with a mean effect difference of −22%. Low boundary layer height and weak ventilation favored $PM_{2.5}$ accumulation, whereas stronger winds and higher boundary layers promoted pollutant dispersion and removal.[3].

2. The response of $PM_{2.5}$ to meteorological variability showed clear spatial heterogeneity. Northern Henan cities, such as Anyang, Hebi, and Xinxiang, exhibited high meteorological sensitivity, while central Henan showed moderate sensitivity and southern Henan showed relatively low sensitivity. This spatial difference reflects the combined effects of the terrain, city location, regional transport, and emission background. Therefore, meteorological effects on $PM_{2.5}$ should be interpreted not only from the provincial mean perspective but also from the perspective of city-level sensitivity.

3. Different meteorological backgrounds further reshaped regional transport pathways and source-contribution structures. In 2020, stagnant conditions and a lower boundary layer favored local accumulation and near-range transport, with important contributions from Beijing–Tianjin–Hebei, Shandong, and Shanxi. In 2023, stronger dispersion and changed airflow patterns weakened the influence of traditional northern source regions and increased the relative importance of Anhui and Hubei.

4. Meteorological variability reshaped the dominant pollution mechanisms. The 2020 episode represented a local accumulation regime, characterized by rapid $PM_{2.5}$ growth, a higher peak, longer persistence, and slower dissipation under stagnant conditions. In contrast, the 2023 episode represented a regional transport regime, in which overall $PM_{2.5}$ concentrations were lower but external transport from surrounding provinces became relatively more important. Primary and secondary $PM_{2.5}$ responded differently to meteorological changes. Primary $PM_{2.5}$ was more sensitive to wind fields, transport pathways, and near-source accumulation, while secondary $PM_{2.5}$ showed a more regionally mixed and stable source structure due to precursor transport and chemical transformation.

This study provides new insight into the meteorology-driven transformation of winter $PM_{2.5}$ pollution regimes in Henan Province. Instead of only describing $PM_{2.5}$ concentration changes, this study links meteorological variability with transport-pathway shifts, source-contribution structures, and stage-dependent pollution evolution. The findings suggest that winter $PM_{2.5}$ control should distinguish between local accumulation, regional transport, and secondary formation under different meteorological regimes. For northern Henan, emission reduction remains crucial during stagnant periods, while for central and southern Henan, regional joint control should pay more attention to changing transport pathways from surrounding provinces.

Although the model validation results indicate that the WRF-CMAQ system reasonably reproduced the main meteorological variables and pollutant variations, several uncertainties and errors should still be acknowledged. First, city-level mean concentrations may be affected by the spatial representativeness of monitoring sites. Second, meteorological simulation biases, especially those related to boundary layer height, wind speed, wind direction, and relative humidity, may introduce uncertainties into the simulation of $PM_{2.5}$ dispersion, transport, accumulation, and secondary formation processes. Third, uncertainties in the emission inventory and the use of a fixed 2020 emission inventory may affect the quantified meteorological effects. Finally, assumptions in the CMAQ source-tagging

method regarding various processes such as precursor tagging and chemical transformation may affect the calculation of source contributions.

Supplementary Materials: The following supporting information can be downloaded at https://www.mdpi.com/article/10.3390/atmos17050502/s1. Table S1. Formulas for Statistical Metrics in Model Validation. Table S2. Model inputs and validation parameters: meteorological elements (2020, 2023) and pollutants (2020). Table S3. Interannual variations and mean effect differences of simulated $PM_{2.5}$ concentrations in January from 2015 to 2025. Table S4. Contributions of emission and meteorological impacts and changes in $PM_{2.5}$ concentrations across 17 prefecture-level cities in Henan Province. Table S5. Regional contributions to $PM_{2.5}$ concentrations (2020, 2023). Table S6. Key parameter settings for the WRF model [60–65]; Table S7. Structure of the CMAQ system used in this study; Figure S1. Modeling domain. Figure S2. Comparison of modeled and observed meteorological data in Henan Province (January 2020 and January 2023). Figure S3. Bar chart of mean effect differences across cities in Henan Province from 2015 to 2025. Figure S4. Bar chart of mean effect differences across cities in Henan Province from 2015 to 2025 (continued). Figure S5. Vertical profiles of (a) wind speed (WS) and (b) vertical wind shear (VWS) during typical heavy pollution episodes (2020, 2023).

Author Contributions: Investigation, Y.H., Y.Y. and F.S.; data curation, Y.H. and X.L. (Xiawen Lei).; writing—original draft, Y.H.; writing—review and editing, F.S., X.L. (Xiaoyong Liu). and R.Z. All authors have read and agreed to the published version of the manuscript.

Funding: This work was supported by the Scientific Research Foundation for the Key R&D Project of Henan Province (No. 262102321044) and National Key R&D Program of China (No. 2024YFC3713700).

Institutional Review Board Statement: Not applicable.

Informed Consent Statement: Not applicable.

Data Availability Statement: Data are contained within the article.

Acknowledgments: The authors thank the Supercomputing Center of Zhengzhou University and Henan Province Supercomputing Center (http://nscc.zzu.edu.cn/, accessed on 16 April 2026) for providing computing resources.

Conflicts of Interest: The research was conducted in the absence of any commercial or financial relationships that could be construed as a potential conflict of interest.

References

1. Abriha-Molnár, V.É.; Szabó, S.; Magura, T.; Tóthmérész, B.; Abriha, D.; Sipos, B.; Simon, E. Environmental impact assessment based on particulate matter, and chlorophyll content of urban trees. *Sci. Rep.* **2024**, *14*, 70664. [CrossRef]
2. Cohen, A.; Brauer, M.; Burnett, R. Estimates and 25-year trends of the global burden of disease attributable to ambient air pollution: An analysis of data from the Global Burden of Diseases Study 2015. *Lancet* **2017**, *389*, 1907–1918, Erratum in *Lancet* **2018**, *391*, 1576. [CrossRef] [PubMed]
3. Manisalidis, I.; Stavropoulou, E.; Stavropoulos, A.; Bezirtzoglou, E. Environmental and health impacts of air pollution: A review. *Front. Public Health* **2020**, *8*, 14. [CrossRef]
4. Shi, Q.; Zheng, B.; Zheng, Y.; Tong, D.; Liu, Y.; Ma, H.; Hong, C.; Geng, G.; Guan, D.; He, K.; et al. Co-benefits of CO_2 emission reduction from China's clean air actions between 2013–2020. *Nat. Commun.* **2022**, *13*, 41467. [CrossRef] [PubMed]
5. Jiang, Y.; Sun, Y.; Li, S.; Yin, D.; Ding, D.; Dong, Z.; Zheng, H.; Zhao, B.; Wang, S. Differentiated regional impacts of future meteorological changes and anthropogenic emission control on $PM_{2.5}$ concentrations in China. *Sustain. Horiz.* **2025**, *16*, 100151. [CrossRef]
6. Department of Ecology and Environment of Henan Province. 2024 Henan Provincial Ecological Environment Status Bulletin. 2025. Available online: https://sthjt.henan.gov.cn/ (accessed on 1 April 2026). (In Chinese)
7. Department of Ecology and Environment of Hebei Province. 2024 Hebei Provincial Ecological Environment Status Bulletin. 2025. Available online: https://hbepb.hebei.gov.cn/ (accessed on 1 April 2026). (In Chinese)

8. Department of Ecology and Environment of Shandong Province. 2024 Shandong Provincial Ecological Environment Status Bulletin. 2025. Available online: http://xxgk.sdein.gov.cn/xxgkml/hjzkgb/202506/t20250604_4826392.html (accessed on 1 April 2026). (In Chinese)
9. Liu, Z.; Gao, W.; Yu, Y.; Hu, B.; Xin, J.; Sun, Y. Characteristics of $PM_{2.5}$ mass concentrations and chemical species in urban and background areas of China: Emerging results from the CARE-China network. *Atmos. Chem. Phys.* **2018**, *18*, 8849–8871. [CrossRef]
10. Li, Q.; Zhang, H.; Cai, X.; Song, Y.; Zhu, T. The impacts of the atmospheric boundary layer on regional haze in North China. *npj Clim. Atmos. Sci.* **2021**, *4*, 41612. [CrossRef]
11. Xiao, Q.; Zheng, Y.; Geng, G.; Chen, C.; Huang, X. Separating emission and meteorological contributions to long-term $PM_{2.5}$ trends over eastern China during 2000–2018. *Atmos. Chem. Phys.* **2021**, *21*, 9475–9496. [CrossRef]
12. Hassan, M.; Mehmood, T.; Liu, J.; Luo, X.; Li, X.; Tanveer, M.; Faheem, M.; Shakoor, A.; Dar, A.; Abid, M. A review of particulate pollution over Himalaya region: Characteristics and salient factors contributing ambient PM pollution. *Atmos. Environ.* **2023**, *294*, 119472. [CrossRef]
13. Jia, Z.; Doherty, R.; Ordóñez, C.; Li, C.; Wild, O.; Jain, S.; Tang, X. The impact of large-scale circulation on daily fine particulate matter ($PM_{2.5}$) over major populated regions of China in winter. *Atmos. Chem. Phys.* **2022**, *22*, 6471–6487. [CrossRef]
14. Wang, T.; Du, H.; Zhao, Z.; Russo, A.; Zhang, J.; Zhou, C. The impact of potential recirculation on the air quality of Bohai Bay in China. *Atmos. Pollut. Res.* **2022**, *13*, 101268. [CrossRef]
15. Li, J.; Han, Z.; Wu, Y.; Xiong, Z.; Xia, X.; Li, J.; Liang, L.; Zhang, R. Aerosol radiative effects and feedbacks on boundary layer meteorology and $PM_{2.5}$ chemical components during winter haze events over the Beijing-Tianjin-Hebei region. *Atmos. Chem. Phys.* **2020**, *20*, 8659–8690. [CrossRef]
16. Liu, L.; Long, X.; Li, Y.; Zang, Z.; Wang, F.; Han, Y.; Bao, Z.; Chen, Y.; Feng, T.; Yang, J. Impacts of meteorology and emission reductions on haze pollution during the lockdown in the North China Plain. *Atmos. Chem. Phys.* **2025**, *25*, 1569–1585. [CrossRef]
17. Zheng, G.; Duan, F.; Su, H.; Ma, Y.; Cheng, Y.; Zheng, B.; Zhang, Q. Exploring the severe winter haze in Beijing: The impact of synoptic weather, regional transport and heterogeneous reactions. *Atmos. Chem. Phys.* **2015**, *15*, 2969–2983. [CrossRef]
18. Wang, J.; Han, J.; Li, T.; Wu, T.; Fang, C. Impact analysis of meteorological variables on $PM_{2.5}$ pollution in the most polluted cities in China. *Heliyon* **2023**, *9*, 17609. [CrossRef] [PubMed]
19. Shen, F.; Hegglin, M.; Yuan, Y. Impact of weather patterns and meteorological factors on $PM_{2.5}$ and O_3 responses to the COVID-19 lockdown in China. *Atmos. Chem. Phys.* **2024**, *24*, 6539–6553. [CrossRef]
20. Jain, S.; Doherty, R.; Sexton, D.; Turnock, S.; Li, C.; Jia, Z.; Shi, Z.; Pei, L. Future projections of daily haze-conducive and clear weather conditions over the North China Plain using a perturbed parameter ensemble. *Atmos. Chem. Phys.* **2022**, *22*, 7443–7460. [CrossRef]
21. Liu, J.; Christensen, J.; Ye, Z.; Dong, S.; Geels, C.; Brandt, J.; Nenes, A.; Yuan, Y.; Im, U. Impact of meteorology and aerosol sources on $PM_{2.5}$ and oxidative potential variability and levels in China. *Atmos. Chem. Phys.* **2024**, *24*, 10849–10867. [CrossRef]
22. Shi, Z.; Huang, L.; Li, J.; Ying, Q.; Zhang, H.; Hu, J. Sensitivity analysis of the surface ozone and fine particulate matter to meteorological parameters in China. *Atmos. Chem. Phys.* **2020**, *20*, 13455–13466. [CrossRef]
23. Li, M.; Wang, T.; Xie, M.; Li, S.; Zhuang, B.; Fu, Q.; Zhao, M.; Wu, H.; Liu, J.; Saikawa, E.; et al. Drivers for the poor air quality conditions in North China Plain during the COVID-19 outbreak. *Atmos. Environ.* **2021**, *246*, 118103. [CrossRef]
24. Lv, L.; Wei, P.; Hu, J.; Chen, Y.; Shi, Y. Source apportionment and regional transport of $PM_{2.5}$ during haze episodes in Beijing combined with multiple models. *Atmos. Res.* **2022**, *266*, 105957. [CrossRef]
25. Dai, W.; Zhou, Y.; Wang, X.; Qi, P. Variation characteristics of $PM_{2.5}$ pollution and transport in typical transport channel cities in winter. *Environ. Sci.* **2024**, *45*, 23–35. (In Chinese)
26. Dou, X.; Yu, S.; Li, J.; Sun, Y.; Song, Z.; Yao, N.; Li, P. The WRF-CMAQ simulation of a complex pollution episode with high-level O_3 and $PM_{2.5}$ over the North China Plain: Pollution characteristics and causes. *Atmosphere* **2024**, *15*, 20198. [CrossRef]
27. Wen, W.; He, X.; Ma, X.; Wei, P.; Cheng, S. Understanding the regional transport contributions of primary and secondary $PM_{2.5}$ components over Beijing during a severe pollution episode. *Aerosol Air Qual. Res.* **2018**, *18*, 1720–1733. [CrossRef]
28. Hu, W.; Zhao, T.; Bai, Y.; Shen, L.; Sun, X.; Gu, Y. Contribution of regional $PM_{2.5}$ transport to air pollution enhanced by sub-basin topography: A modeling case over central China. *Atmosphere* **2020**, *11*, 1258. [CrossRef]
29. Sulaymon, I.; Zhang, Y.; Hu, J.; Hopke, P.; Zhang, Y.; Zhao, B.; Xing, J.; Li, L.; Mei, X. Evaluation of regional transport of $PM_{2.5}$ during severe atmospheric pollution episodes in the western Yangtze River Delta, China. *J. Environ. Manag.* **2021**, *293*, 112827. [CrossRef] [PubMed]
30. Wang, Y.; Bai, Y.; Zhi, X.; Wu, K.; Zhao, T. Two typical patterns of regional $PM_{2.5}$ transport for heavy air pollution over central China: Rapid transit transport and stationary accumulation transport. *Front. Environ. Sci.* **2022**, *10*, 890514. [CrossRef]
31. Wang, S.; Zhao, B.; Cai, S.; Klimont, Z.; Nielsen, C.; Morikawa, T.; Woo, J. Emission trends and mitigation options for air pollutants in East Asia. *Atmos. Chem. Phys.* **2014**, *14*, 6571–6603. [CrossRef]
32. Li, K.; Jacob, D.; Liao, H.; Zhu, J.; Shah, V.; Shen, L. A two-pollutant strategy for improving ozone and particulate air quality in China. *Nat. Geosci.* **2019**, *12*, 906–910. [CrossRef]

33. Guo, Q.; He, Z.; Wang, Z. The Characteristics of Air Quality Changes in Hohhot City in China and their Relationship with Meteorological and Socio-economic Factors. *Aerosol Air Qual. Res.* **2024**, *24*, 274. [CrossRef]
34. Qiao, S.; Guo, Q.; He, Z.; Feng, G.; Wang, Z.; Li, X. Spatiotemporal Trends and Drivers of $PM_{2.5}$ Concentrations in Shandong Province from 2014 to 2023 Under Socioeconomic Transition. *Toxics* **2025**, *13*, 978. [CrossRef]
35. Song, Q.; Huang, L.; Zhang, Y.; Li, Z.; Wang, S. Driving Factors of $PM_{2.5}$ Pollution Rebound in North China Plain in Early 2023. *Environ. Sci. Technol. Lett.* **2025**, *12*, 305–312. [CrossRef]
36. Silver, B.; Reddington, C.; Chen, Y.; Arnold, S. A decade of China's air quality monitoring data suggests health impacts are no longer declining. *Environ. Int.* **2025**, *197*, 109318. [CrossRef] [PubMed]
37. Lin, C.; Huang, R.; Duan, J.; Qu, J.; Liu, J. Growing role of secondary organic aerosol in the North China Plain from 2014 to 2024. *Atmos. Chem. Phys.* **2026**, *26*, 2635–2647. [CrossRef]
38. Chen, X.; Li, X.D.; Liang, J.; Li, X.; Li, S.; Chen, G.; Chen, Z.; Dai, S.; Bin, J.; Tang, Y. Causes of the unexpected slowness in reducing winter $PM_{2.5}$ for 2014–2018 in Henan Province. *Environ. Pollut.* **2023**, *319*, 120928. [CrossRef]
39. He, J.; Xue, W.; Yan, L.; Shi, Y.; Wang, Y.; Lei, Y.; Zheng, Y.; Zhang, Y. Multi-dimensional sources apportionment of $PM_{2.5}$ in Zhongyuan urban agglomeration based on the CAMx model. *Aerosol Air Qual. Res.* **2022**, *22*, 210254. [CrossRef]
40. Zhao, Y.; Wang, K.; Liu, X.; Xu, Q.; Luo, L.; Liu, P.; He, Y.; Yu, Y.; Su, F.; Zhang, R. Characteristics and driving factors of $PM_{2.5}$ concentration changes in central China. *Atmosphere* **2025**, *16*, 1227. [CrossRef]
41. Wang, M.; Cao, L.; Xu, L.; Wang, Y.; Kong, H.; Gao, M.; Qin, Y.; Meng, K. Characteristics and influencing factors of $PM_{2.5}$-O_3 composite pollution in Henan Province. *Environ. Sci.* **2025**, *46*, 1285–1301. (In Chinese)
42. Kalnay, E.; Kanamitsu, M.; Kistler, R.; Collins, W.; Deaven, D.; Gandin, L.; Iredell, M.; Saha, S. The NCEP/NCAR 40-year reanalysis project. *Bull. Am. Meteorol. Soc.* **1996**, *77*, 437–471. [CrossRef]
43. Wang, Y.; Wang, X.; Liu, Z.; Chao, S.; Zhang, J.; Zheng, Y.; Zhang, Y.; Xue, W.; Wang, J.; Lei, Y. Assessing the effectiveness of $PM_{2.5}$ pollution control from the perspective of interprovincial transport and $PM_{2.5}$ mitigation costs across China. *Environ. Sci. Ecotechnol.* **2024**, *22*, 100448. [CrossRef]
44. Guenther, A.; Jiang, X.; Heald, C.; Sakulyanontvittaya, T.; Duhl, T.; Emmons, L.; Wang, X. The Model of Emissions of Gases and Aerosols from Nature version 2.1 (MEGAN2.1): An extended and updated framework for modeling biogenic emissions. *Geosci. Model. Dev.* **2012**, *5*, 1471–1492. [CrossRef]
45. Zeren, Y.; Zhou, B.; Zheng, Y.; Jiang, F.; Lyu, X.; Xue, L.; Wang, H.; Liu, X.; Guo, H. Does ozone pollution share the same formation mechanisms in the Bay Areas of China? *Environ. Sci. Technol.* **2022**, *56*, 14326–14337. [CrossRef]
46. Su, F.; Xu, Q.; Wang, K.; Yin, S.; Wang, S.; Zhang, R.; Tang, X.; Ying, Q. On the effectiveness of short-term intensive emission controls on ozone and particulate matter in a heavily polluted megacity in central China. *Atmos. Environ.* **2021**, *246*, 118111. [CrossRef]
47. Ying, Q.; Zhang, J.; Zhang, H.; Hu, J.; Kleeman, M. Atmospheric age distribution of primary and secondary inorganic aerosols in a polluted atmosphere. *Environ. Sci. Technol.* **2021**, *55*, 5668–5676. [CrossRef]
48. Xie, X.; Ying, Q.; Zhang, H.; Hu, J. Spatial and temporal variations in the atmospheric age distribution of primary and secondary inorganic aerosols in China. *Engineering* **2023**, *28*, 117–129. [CrossRef]
49. Ying, Q.; Feng, M.; Song, D.; Wu, L.; Hu, J.; Zhang, H.; Kleeman, M.; Li, X. Improve regional distribution and source apportionment of $PM_{2.5}$ trace elements in China using inventory-observation constrained emission factors. *Sci. Total Environ.* **2018**, *624*, 355–365. [CrossRef]
50. Hammer, M.; van Donkelaar, A.; Martin, R.; McDuffie, E.; Lyapustin, A.; Sayer, A.; Hsu, N.; Levy, R.; Garay, M.; Kalashnikova, O.; et al. Effects of COVID-19 lockdowns on fine particulate matter concentrations. *Sci. Adv.* **2021**, *7*, 7670. [CrossRef] [PubMed]
51. Wang, N.; Xu, J.; Pei, C.; Tang, R.; Zhou, D.; Chen, Y.; Li, M.; Deng, X.; Deng, T.; Huang, X.; et al. Air quality during COVID-19 lockdown in the Yangtze River Delta and the Pearl River Delta: Two different responsive mechanisms to emission reductions in China. *Environ. Sci. Technol.* **2021**, *55*, 5721–5730. [CrossRef] [PubMed]
52. Emery, C.; Tai, E. *Enhanced Meteorological Modeling Performance Evaluation for Two Texas Ozone Episodes*; Environmental International Corporation: Novato, CA, USA, 2001.
53. English, S.; McNally, A.; Bormann, N.; Salonen, K.; Matricardi, M.; Horanyi, A.; Rennie, M.; Janisková, M.; Di Michele, S.; Geer, A.; et al. *Impact of Satellite Data*; European Centre for Medium-Range Weather Forecasts: Reading, UK, 2013.
54. Boylan, J.; Russell, A. PM and light extinction model performance metrics, goals, and criteria for three-dimensional air quality models. *Atmos. Environ.* **2006**, *40*, 4946–4959. [CrossRef]
55. Sun, J.; Xie, X.; Qin, M.; Yu, X.; Ji, D.; Gong, K.; Li, J.; Huang, L.; Hu, J. Analysis of coordinated relationship between $PM_{2.5}$ and ozone and its affecting factors ondifferent timescales. *Chin. Sci. Bull.* **2022**, *67*, 2018–2028. [CrossRef]
56. Li, Y.; He, J.; Ren, Y.; Wang, H. Aerosol-PBL relationship under diverse meteorological conditions: Insights from satellite/radiosonde measurements in North China. *Atmos. Res.* **2025**, *321*, 108125. [CrossRef]

57. Li, M.; Wang, L.; Liu, J.; Gao, W.; Song, T.; Sun, Y.; Li, L.; Li, X.; Wang, Y.; Liu, L.; et al. Exploring the regional pollution characteristics and meteorological formation mechanism of $PM_{2.5}$ in North China during 2013–2017. *Environ. Int.* **2020**, *134*, 105283. [CrossRef] [PubMed]
58. Huang, A.; Cheng, W.; Chu, M.; Wang, G.; Yang, H.; Zhang, L. A comprehensive attribution analysis of $PM_{2.5}$ in typical industrial cities during the winter of 2016–2018: Effect of meteorology and emission reduction. *Atmos. Res.* **2024**, *299*, 107181. [CrossRef]
59. Gong, D.; Du, N.; Wang, L.; Deng, X.; Zhang, X.; Yang, L. Impacts of meteorological and precursor emission factors on $PM_{2.5}$ and O_3 from 2019 to 2022: Insights from multiple perspectives. *Atmos. Res.* **2025**, *315*, 107933. [CrossRef]
60. Lin, Y.; Farley, R.; Orville, H. Bulk Parameterization of the Snow Field in a Cloud Model. *J. Clim. Appl. Meteorol.* **1983**, *22*, 1065–1092. [CrossRef]
61. Mlawer, E.J.; Taubman, S.J.; Brown, P.D.; Iacono, M.J.; Clough, S.A. Radiative transfer for inhomogeneous atmospheres: RRTM, a validated correlated-k model for the longwave. *J. Geophys. Res.-Atmos.* **1997**, *102*, 16663–16682. [CrossRef]
62. Chen, F.; Janjic, Z.; Mitchell, K. Impact of atmospheric surface-layer parameterizations in the new land-surface scheme of the NCEP mesoscale Eta model. *Bound.-Layer Meteorol.* **1997**, *85*, 391–421. [CrossRef]
63. Salamanca, F.; Krpo, A.; Martilli, A.; Clappier, A. A new building energy model coupled with an urban canopy parameterization for urban climate simulations-part I. formulation, verification, and sensitivity analysis of the model. *Theor. Appl. Climatol.* **2010**, *99*, 331–344. [CrossRef]
64. Janjic, Z. The Step-Mountain Eta Coordinate Model–Further Developments of the Convection, Viscous Sublayer, and Turbulence Closure Schemes. *Mon. Weather. Rev.* **1994**, *122*, 927–945. [CrossRef]
65. Grell, G.; Dévényi, D. A generalized approach to parameterizing convection combining ensemble and data assimilation techniques -: Art. no. 1693. *Geophys. Res. Lett.* **2002**, *29*, 1693. [CrossRef]

Disclaimer/Publisher's Note: The statements, opinions and data contained in all publications are solely those of the individual author(s) and contributor(s) and not of MDPI and/or the editor(s). MDPI and/or the editor(s) disclaim responsibility for any injury to people or property resulting from any ideas, methods, instructions or products referred to in the content.